Langmuir
Article
pubs.acs.org/Langmuir

General Strategy for Designing Functionalized Magnetic Microspheres for Different Bioapplications

Xinglu Huang,[†,∥] Jie Zhuang,[‡,∥] Dong Chen,[†,§] Huiyu Liu,[†] Fangqiong Tang,*[,†] Xiyun Yan,[‡] Xianwei Meng,[†] Lin Zhang,[†] and Jun Ren[†]

[†]*Laboratory of Controllable Preparation and Application of Nanomaterials, Technical Institute of Physics and Chemistry, Chinese Academy of Sciences, Beijing 100190, China,* [‡]*National Laboratory of Biomacromolecules, and China-Japan Joint Laboratory of Structural Virology and Immunology, Institute of Biophysics, Chinese Academy of Sciences, Beijing 100101, China,* [§]*Beijing Creative Nanophase Hi-Tech Company, Limited, Beijing 100086, China, and* [∥]*Graduate School of the Chinese Academy of Sciences, Beijing 100049, China*

Received April 9, 2009. Revised Manuscript Received July 30, 2009

Surface functionalization and water solubility of magnetic nanoparticles are crucial for bioapplication. Here, we describe a synthetic approach for direct preparation of a wide range of functionalized and hydrophilic magnetic polymer particles (MPPs) that is both simple and general and involves using different polymers as the source of functional groups. This simple strategy of changing the polymer used in the reaction can give rise to a wide variety of hydrophilic MPPs with a high number of functional groups. For the purpose of bioapplication, we synthesized three types of MPPs with typical functional groups, such as hydroxyl groups (−OH), amino groups ($-NH_2$), and carboxyl groups (−COOH), and further characterized these MPPs by transmission electronic microscopy (TEM), scanning electronic microscopy (SEM), thermogravimetric analysis (TGA), X-ray powder diffraction (XRD), Raman spectroscopy, and Fourier transform infrared (FTIR) spectroscopy. The magnetic saturation of the MPPs was also studied and was adequate for most bioapplications. MPPs were shown to have good biocompatibility using cell proliferation and apoptosis assays. Two types of MPPs with different functional groups were used successfully for intracellular imaging and antibody purification. Our results demonstrate that this simple and general synthesis strategy has potential for designing hydrophilic magnetic nanoparticles with multifunctionalities that cater for a range of bioapplications.

Introduction

The functional groups on the surfaces of nanoparticles are important for bioapplications and need to be suitable for conjugation with biomolecules, such as enzymes, antibodies, and nucleotides. Even though surface modifications are a feasible strategy for nanoparticle functionalization, some surface modifications can make magnetic nanoparticles (MNPs) unstable and prone to aggregation or cytotoxicity, resulting in poor biocompatibility.[1] The density of the resulting functional groups on nanoparticle surfaces is also difficult to control because of unstable modification efficiency. In recent years, inorganic−organic hybrid nanoparticles with a high number of functional groups, such as MNPs coated in organic macromolecules,[2−5] quantum dots embedded in polymeric structures,[6−8] and silica particles modified by polymers,[9,10] have been investigated as potential nanocarriers because they exhibit wide bioapplications. Hydrophilic magnetic polymer particles (MPPs) have also attracted great attention on account of their potential superiority in the field of biomedicine, especially for applications, such as biomolecular separations,[11] drug delivery,[12−15] biomedical diagnostic agents,[16−18] intracellular imaging,[19,20] and magnetic resonance imaging (MRI).[21−23] The surface of MPPs has a high number of polymer functional groups, making them suitable for further multifunctionalization by attachment of various bioactive molecules.

*To whom correspondence should be addressed. Fax: (+86)10-82543521. E-mail: tangfq@mail.ipc.ac.cn.

(1) Laurent, S.; Forge, D.; Port, M.; Roch, A.; Robic, C.; Vander Elst, L.; Muller, R. N. *Chem. Rev.* **2008**, *108*, 2064–2110.
(2) Lee, H.; Lee, E.; Kim do, K.; Jang, N. K.; Jeong, Y. Y.; Jon, S. *J. Am. Chem. Soc.* **2006**, *128*, 7383–7389.
(3) Pan, X.; Guan, J.; Yoo, J. W.; Epstein, A. J.; Lee, L. J.; Lee, R. J. *Int. J. Pharm.* **2008**, *358*, 263–270.
(4) Guo, J.; Yang, W.; Deng, Y.; Wang, C.; Fu, S. *Small* **2005**, *1*, 737–743.
(5) Petri-Fink, A.; Steitz, B.; Finka, A.; Salaklang, J.; Hofmann, H. *Eur. J. Pharm. Biopharm.* **2008**, *68*, 129–137.
(6) Esteves, A. C.; Bombalski, L.; Trindade, T.; Matyjaszewski, K.; Barros-Timmons, A. *Small* **2007**, *3*, 1230–1236.
(7) Fernandez-Arguelles, M. T.; Yakovlev, A.; Sperling, R. A.; Luccardini, C.; Gaillard, S.; Medel, A. S.; Mallet, J. M.; Brochon, J. C.; Feltz, A.; Oheim, M.; Parak, W. J. *Nano Lett.* **2007**, *7*, 2613–2617.
(8) Mancini, M. C.; Kairdolf, B. A.; Smith, A. M.; Nie, S. *J. Am. Chem. Soc.* **2008**, *130*, 10836–10837.
(9) Jang, J.; Kim, Y. *Chem. Commun.* **2008**, 4016–4018.
(10) Ueno, K.; Inaba, A.; Kondoh, M.; Watanabe, M. *Langmuir* **2008**, *24*, 5253–5259.
(11) Li, Y. C.; Lin, Y. S.; Tsai, P. J.; Chen, C. T.; Chen, W. Y.; Chen, Y. C. *Anal. Chem.* **2007**, *79*, 7519–7525.
(12) Mykhaylyk, O.; Antequera, Y. S.; Vlaskou, D.; Plank, C. *Nat. Protoc.* **2007**, *2*, 2391–2411.
(13) Park, H.; Yang, J.; Seo, S.; Kim, K.; Suh, J.; Kim, D.; Haam, S.; Yoo, K. H. *Small* **2008**, *4*, 192–196.
(14) Yang, J.; Lee, C. H.; Ko, H. J.; Suh, J. S.; Yoon, H. G.; Lee, K.; Huh, Y. M.; Haam, S. *Angew. Chem., Int. Ed.* **2007**, *46*, 8836–8839.
(15) Yoon, T. J.; Kim, J. S.; Kim, B. G.; Yu, K. N.; Cho, M. H.; Lee, J. K. *Angew. Chem., Int. Ed.* **2005**, *44*, 1068–1071.
(16) Ceyhan, B.; Alhorn, P.; Lang, C.; Schuler, D.; Niemeyer, C. M. *Small* **2006**, *2*, 1251–1255.
(17) Wacker, R.; Ceyhan, B.; Alhorn, P.; Schueler, D.; Lang, C.; Niemeyer, C. M. *Biochem. Biophys. Res. Commun.* **2007**, *357*, 391–396.
(18) Gao, L. Z.; Wu, J. M.; Lyle, S.; Zehr, K.; Cao, L. L.; Gao, D. *J. Phys. Chem. C* **2008**, *112*, 17357–17361.
(19) Lewin, M.; Carlesso, N.; Tung, C. H.; Tang, X. W.; Cory, D.; Scadden, D. T.; Weissleder, R. *Nat. Biotechnol.* **2000**, *18*, 410–414.
(20) Serda, R. E.; Adolphi, N. L.; Bisoffi, M.; Sillerud, L. O. *Mol. Imaging* **2007**, *6*, 277–288.
(21) Tromsdorf, U. I.; Bigall, N. C.; Kaul, M. G.; Bruns, O. T.; Nikolic, M. S.; Mollwitz, B.; Sperling, R. A.; Reimer, R.; Hohenberg, H.; Parak, W. J.; Forster, S.; Beisiegel, U.; Adam, G.; Weller, H. *Nano Lett.* **2007**, *7*, 2422–2427.
(22) Nasongkla, N.; Bey, E.; Ren, J.; Ai, H.; Khemtong, C.; Guthi, J. S.; Chin, S. F.; Sherry, A. D.; Boothman, D. A.; Gao, J. *Nano Lett.* **2006**, *6*, 2427–2430.
(23) Briley-Saebo, K.; Bjornerud, A.; Grant, D.; Ahlstrom, H.; Berg, T.; Kindberg, G. M. *Cell Tissue Res.* **2004**, *316*(3), 315–23.

MNPs embedded in or coated with biodegradable polymer evidently also show lower cytotoxicity and have better biocompatiblilty than inorganic modified MNPs.[24]

Biodegradable polymers are usually introduced into magnetic nanoparticles using two major strategies, namely, surface coating and interior embedding. There are a lot of works on the surface coating of magnetic nanoparticles with dextran,[25] polyethylene glycol (PEG),[26] chitosan,[27,28] as well as other macromolecules,[29,30] but it is difficult to develop a strategy for designing many types of MPPs using a general synthesis method. Although many MPPs have been obtained using interior embedding strategies, they have poor monodispersion and the particle diameter is difficult to control.[31,32] Recently, Deng et al. reported a simple one-pot solvothermal method for the preparation of monodisperse magnetic microspheres with a tunable size range of 200−800 nm using the polymer PEG.[33] Subsequently, Li et al. synthesized amphiphilic and superparamagnetic hollow spheres using a copolymer with the same method.[34] However, the properties of surface functional groups, biocompatibility, and bioapplications of these MPPs were not investigated. Most importantly, the range of polymers that can be used as a source of functional groups on the MPP surface was not addressed, thus restricting their bioapplications.

In this paper, a simple and general strategy was developed for designing MPPs for particular bioapplications involving selection of the polymer used in the one-pot synthesis method on the basis of its functional groups. The resulting MPPs did not require any further modifications. There have only been a few previous reports in the literature of simple strategies for the direct preparation of functionalized MPPs.[35−37] These strategies, however, were not general, and the resulting MPP products were not hydrophilic and designed for bioapplications. Because surface functional groups play a significant role in different bioapplications, we chose three types of MPPs that represent typical functional groups for investigation, namely, dextran magnetic microspheres (DMMs) with hydroxyl groups (−OH), chitosan magnetic microspheres (CMMs) with amino groups ($-NH_2$), and poly(acrylic acid) (PAA) magnetic microspheres (PMMs) with carboxyl groups (−COOH). We characterized these three types of MPPs and demonstrated biocompatibility using cell proliferation and apoptosis assays. Multifunctionalized materials designed for intracellular imaging and antibody purification were obtained by the addition of further functionalized molecules to the functional groups on the MPP surface and, subsequently, evaluated.

Experimental Methods

Chemicals. Sodium acetate (NaAc), ethanol, iron chloride ($FeCl_3 \cdot 6H_2O$), ethylene alcohol, chitosan, polyvinyl butyral, polyvinyl alcohol, polyvinyl pyrrolidone, and polyethylene glycol were obtained from Beijing Chemical Reagents Company (China). Annexin V detection kits were purchased from BD (Becton, Dickinson, and Company). Dulbecco's modified Eagle's medium (DMEM) and born calf serum were from GIBCO. 3-(4,5-Dimethylthiazolyl-2)-2,5-diphenyltetrazolium bromide (MTT), dextran, and poly(acrylic acid) (PAA) were purchased from Sigma-Aldrich.

Synthesis and Characterization of MPPs. MPPs were synthesized according to the hydrothermal method.[33] Briefly, $FeCl_3 \cdot 6H_2O$ (0.125 M) was dissolved in ethylene glycol, followed by the addition of NaAc (1 M) and a polymer, such as dextran, chitosan, or PAA (0.2 g). The mixture was stirred vigorously for 30 min, then sealed in an autoclave, and heated at 200 °C for 8−30 h. The products were collected by washing several times with ethanol and then dried at 60 °C.

The crystal structures of samples were characterized by XRD using a Japan D/MAX-RB diffractometer. Morphology and structure images were observed with a JEOL-200CX transmission electron microscope (TEM) and a S-4300 scanning electron microscope (SEM). The content of iron elements in MPPs was measured by SEM spectrum analysis. Thermalgravimetric analysis (TGA) was carried out on a Diamond TG/DTA thermal gravimetric analyzer at a heating rate of 10 °C min^{-1} under an air atmosphere. A vibrating-sample magnetometer (VSM, LDJ-9600) was used to study the magnetic properties of the particles. Raman spectroscopy was recorded on a confocal laser micro-Raman spectroscope (inVia-Reflex, Renishaw). Fourier transform infrared (FTIR) spectra were analyzed by Jasco FT/IR-300E. The sizes of magnetic materials were also measured at 25 °C with a Zetasizer 3000HSA (Malvern).

Cell Culture and Preparation. A375 human malignant melanoma cells (A375 cells) were grown as a monolayer in a humidified incubator in a 95% air/5% CO_2 atmosphere at 37 °C in a dish containing DMEM (GIBCO) supplemented with 10% (v/v) heat-inactivated fetal bovine serum (GIBCO), 100 IU/mL penicillin (GIBCO), and 100 IU/mL streptomycin (GIBCO). A375 cells were detached mechanically and adjusted to the required concentration of viable cells as determined by counting in a hemocytometer.

Intracellular Imaging of CMMs in A375 Cells. Fluoresceinisothiocynate (FITC) was attached to the amine groups of CMMs. CMMs were resuspended in 3 mL of phosphate buffer solution (PBS, pH 8.7) and mixed with a solution of 100 μg/mL FITC. The suspension was stirred overnight, and the FITC-labeled CMMs were collected with a magnet. A total of 1 mg of FITC-labeled CMMs was diluted in 2 mL of DMEM and sterilized. Detached A375 cells were first cultured for 16 h and then incubated for 4 h with the FITC-labeled CMMs. The medium was then replaced by PBS (pH 7.0). Images of the cells were observed under a FV500 confocal laser scanning microscope.

The pH-sensitive fluorescent indicator LysoTracker Blue DND-22 (100 nM, Invitrogen) was added to the A375 cells incubated with 1 mg of FITC-labeled CMMs and incubated for 2 h at 37 °C to label endolysosomal compartments during the uptake of FITC-labeled CMMs. After washing with PBS, cells were imaged with a FV500 confocal laser scanning microscope.

Labeling of PMMs with Protein A and Antibody Purification. PMMs were covalently labeled with protein A. 1-Ethyl-3-(3-dimethly aminopropyl)carbodiimide (EDC, 2 mM), *N*-hydroxysuccinimide (NHS, 5 mM), and deionized water were mixed and vortexed. PMMs (10 mg) were added to the mixing solution and incubated at room temperature for 30 min, then collected by a

(24) Lu, A. H.; Salabas, E. L.; Schuth, F. *Angew. Chem., Int. Ed.* **2007**, *46*, 1222–1244.
(25) Wilhelm, C.; Billotey, C.; Roger, J.; Pons, J. N.; Bacri, J. C. *Biomaterials* **2003**, *24*, 1001–1011.
(26) Veiseh, O.; Sun, C.; Gunn, J.; Kohler, N.; Gabikian, P.; Lee, D.; Bhattarai, N.; Ellenbogen, R.; Sze, R.; Hallahan, A.; Olson, J.; Zhang, M. Q. *Nano Lett.* **2005**, *5*, 1003–1008.
(27) Li, G. Y.; Jiang, Y. R.; Huang, K. L.; Ding, P.; Chen, J. *J. Alloys Compd.* **2008**, *466*, 451–456.
(28) Li, L. L.; Chen, D.; Zhang, Y. Q.; Deng, Z. T.; Ren, X. L.; Meng, X. W.; Tang, F. Q.; Ren, J.; Zhang, L. *Nanotechnology* **2007**, 18.
(29) Lee, H.; Yu, M. K.; Park, S.; Moon, S.; Min, J. J.; Jeong, Y. Y.; Kang, H. W.; Jon, S. *J. Am. Chem. Soc.* **2007**, *129*, 12739–12745.
(30) Ditsch, A.; Laibinis, P. E.; Wang, D. I. C.; Hatton, T. A. *Langmuir* **2005**, *21*, 6006–6018.
(31) Iida, H.; Takayanagi, K.; Nakanishi, T.; Osaka, T. *J. Colloid Interface Sci.* **2007**, *314*, 274–280.
(32) Liang, S.; Wang, Y.; Yu, J.; Zhang, C.; Xia, J.; Yin, D. *J. Mater. Sci.: Mater. Med.* **2007**, *18*, 2297–2302.
(33) Deng, H.; Li, X.; Peng, Q.; Wang, X.; Chen, J.; Li, Y. *Angew. Chem., Int. Ed.* **2005**, *44*, 2782–2785.
(34) Li, X. H.; Zhang, D. H.; Chen, J. S. *J. Am. Chem. Soc.* **2006**, *128*, 8382–8383.
(35) Li, Z.; Tan, B.; Allix, M.; Cooper, A. I.; Rosseinsky, M. J. *Small* **2008**, *4*, 231–239.
(36) Liu, H. B.; Guo, J.; Jin, L.; Yang, W. L.; Wang, C. C. *J. Phys. Chem. B* **2008**, *112*, 3315–3321.
(37) Guan, N. N.; Liu, C.; Sun, D. J.; Xu, J. *Colloids Surf., A* **2009**, *335*, 174–180.

magnet, and washed twice with deionized water. Functionalized PMMs were added to a solution of protein A (1 mg/mL) and NaAc buffer (pH 6.0, 0.2 M) and vortexed, and the mixture was incubated at 4 °C for 2 h. The protein-A-labeled PMMs were collected with a magnet, washed twice with PBS (pH 7.0), and incubated in Tris buffer (pH 7.5, 50 mM) at room temperature for 30 min. Protein-A-labeled PMMs were then purified and dispersed into a PBS solution. The concentration of protein A in the supernatant before and after labeling was measured, and the labeling efficiency was calculated as the ratio of free to labeled protein A.

The activity of protein A attached to PMMs was detected: first, HRP-labeled goat-anti-mouse IgG was added to PBS containing protein-A-labeled PMMs and incubated for 30 min. BSA-blocked naked PMMs were used as a negative control. Then, HRP-antibody-protein A-labeled PMMs were separated with a magnet, and the HRP substrate TMB was added in the presence of H_2O_2 producing a blue color. The color reaction was quenched by adding H_2SO_4 and measured at 450 nm using a Hitachi UV2010 spectrophotometer.

Antibody purification by protein-A-labeled PMMs. Ascites were diluted in PBS and then incubated with protein-A-labeled PMMs at 4 °C for 2 h. Antibody-labeled PMMs were then collected with a magnet and washed twice with PBS. Antibody was eluted from the multifunctionalized PMMs by Gly-HCl (pH 3.0, 50 mM) and dialyzed 3 times with PBS.

Effect of MPPs on A375 Cells. Cytotoxicity of three types of MPPs synthesized here was evaluated using the MTT cell viability assay. First, A375 cells were cultured at a density of 8000 cells per well in 96-well plates and incubated with different concentrations of MPPs for 24 h. The viability of the A375 cells was subsequently determined using a MTT proliferation assay kit.

Cell apoptosis was determined with a fluorescence activated cell sorter (FACS) and assessed with an annexin V detection kit. After incubation with MPPs for 24 h, A375 cells were stained with annexin V and PI and assessed by FACS as described previously.[38] Briefly, cells were washed with binding buffer and incubated with annexin V and PI at room temperature for 10 min and then analyzed immediately by FACS.

Results and Discussion

Preparation and Structure of MPPs. Nine MPPs with different types of functional groups were synthesized using different polymers as surfactants in the one-pot hydrothermal method. The particles were characterized by TEM and showed excellent monodispersion (Supplemental Figure 1 in the Supporting Information). To achieve a high number of functional groups exposed on the surfaces of MPPs, we chose polymers that were synthesized from monomers carrying functional groups suited for the attachment of the bioactive molecules required for particular bioapplications. Here, we selected three MPPs with common functional groups for further investigation, namely, DMMs with −OH, CMMs with $-NH_2$, and PMMs with −COOH. DMMs, CMMs, and PMMs were all spherical and uniform in size (about 430 nm) (Figure 1). The size of MPPs was controlled to within a range of 200−800 nm by adjusting the reaction time and the concentration of Fe^{3+} and NaAc. In agreement with a previous report,[39] we found no obvious linear correlation between the particle size and reaction time or concentration of reactants; however, it was clear that particle size increased with increasing concentrations of Fe^{3+} and longer reaction times (Supplemental Table 1 in the Supporting Information). For example, 330 nm DMMs were produced with reactant concentrations of 0.125 M $FeCl_3$ and 1 M NaAc and a reaction time of 8 h, while 660 nm particles were obtained by increasing the concentrations of the reactants to 0.25 M $FeCl_3$ and 1.5 M NaAc and the reaction time to 20 h. The relationship between the quantity of polymer used in the reaction and reaction time also played an important role in the monodispersion of MPPs. DMMs, for example, were cross-linked with excess polymer when the quantity of the polymer used was 0.5 g and the reaction time was 8 h (Supplemental Figure 2A in the Supporting Information). However, monodispersion of particles was better when the quantity of polymer used was 0.5 g and the reaction time was 20 h (Supplemental Figure 2B in the Supporting Information). As with the correlation of particle size and reaction time or concentration of reactants, there was no obvious linear correlation between the quantity of polymer and reaction time in the monodispersion of MPPs.

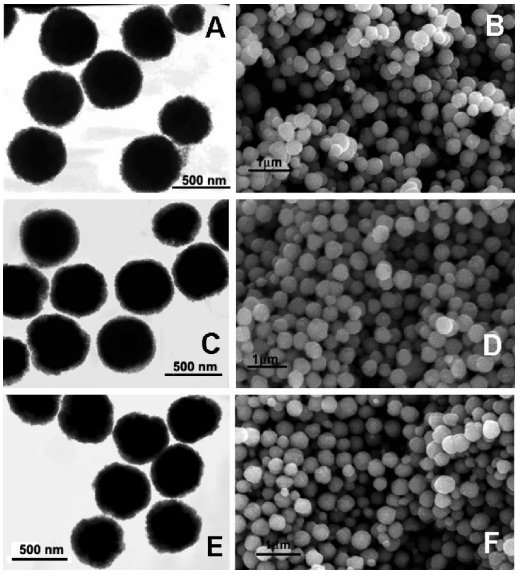

Figure 1. TEM and SEM images of three types of MPPs. TEM images of (A) DMMs (460 nm), (C) CMMs (430 nm), and (E) PMMs (480 nm). SEM images of (B) DMMs, (D) CMMs, and (F) PMMs.

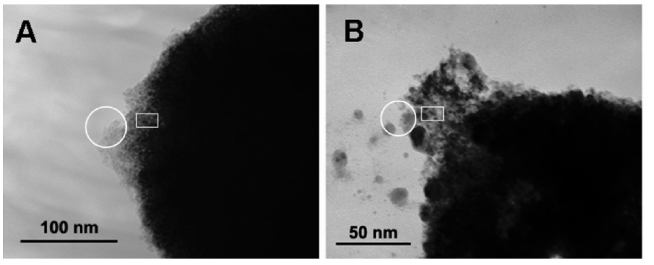

Figure 2. Analysis of MPPs structure. (A) Representative TEM image of MPPs not treated with HCl (size ≈ 460 nm). (B) Representative TEM image of MPPs treated with HCl (size ≈ 320 nm).

The TGA analysis was employed to confirm the existence of polymers in/on the microspheres. Three types of MPPs were heated to 240 °C, and results showed that the mass of microspheres occurred about 30% decreasing attributed to the degradation of polymers (Figure 3A). To gain a better understanding of the structure of MPPs, the MPPs were eroded by incubation in 0.1 M HCl for 30 min. When representative TEM images of untreated Fe_3O_4 microspheres (Figure 2A) and treated microspheres (Figure 2B) are compared, it can be seen that small magnetic nanocrystals (boxed area, about 5−20 nm) are assembled

(38) Huang, X. L.; Meng, X. W.; Tang, F. Q.; Li, L. L.; Chen, D.; Liu, H. Y.; Zhang, Y. Q.; Ren, J. *Nanotechnology* **2008**, 19.
(39) Zhang, H.; Zhong, X.; Xu, J. J.; Chen, H. Y. *Langmuir* **2008**, *24*, 13748–13752.

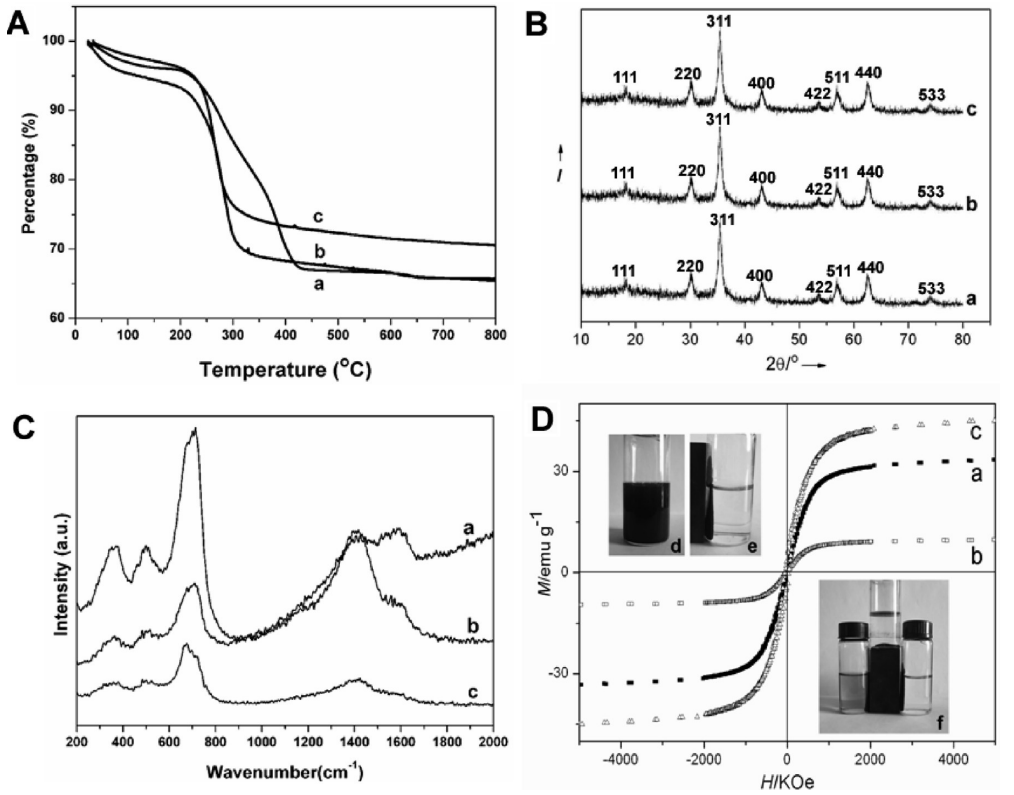

Figure 3. TGA, X-ray diffractograms, Raman spectroscopy, and magnetization curves of three types of MPPs. (A) TGA curves, (B) X-ray diffractograms, and (C) Raman spectra of (a) dextan, (b) chitosan, and (c) PAA magnetic microspheres. (D) Magnetization curves of (a) dextran, (b) chitosan, and (c) PAA magnetic microspheres. (d) Nanocrystals are easily dispersed in water and (e and f) can be drawn from the solution to the sidewall of the vial by a magnetic field.

together in the microspheres by polymer (circled area). Our experimental results are consistent with other reports[34] and indicate that polymers are present at both the surface and in the interior of the microspheres. In our one-pot synthesis reactions, the role of each reactant was as follows: ethylene glycol is known from the polyol process to produce monodisperse metal or metal oxide nanoparticles and was used here as a high-boiling-point reducing agent; sodium acetate was used as an electrostatic stabilizer to prevent particle agglomeration; and different polymers were used as surfactants to prevent particle agglomeration and play a role in the assembly of inorganic nanocrystals in the microspheres.[39]

Characterization of MPPs. Figure 3B represented the XRD pattern of three types of MPPs, which were identical with that of γ-Fe_2O_3 and Fe_3O_4.[40] However, because of the very similar patterns of these two forms of MPPs, the XRD pattern could not provide enough evidence to conclude that the MPPs were γ-Fe_2O_3 or Fe_3O_4. Micro-Raman spectra were carried out to further investigate the crystalline form of MPPs (Figure 3C). All of the three types of MPPs had two peaks centered at the wavelengths of around 1430 and 1580 cm^{-1}, which were attributed to the γ-Fe_2O_3 phase.[41] The broadened peak over the wavelength 600−800 cm^{-1} was also a characteristic band of γ-Fe_2O_3. There was no peak at 663 cm^{-1}, a typical peak of Fe_3O_4.[41] TGA curves of the three types of MPPs determined in air flow (Figure 3A) did not show any increasing of the mass of MPPs above 400 °C. This revealed that there was no Fe_3O_4 in the product, which should transform to

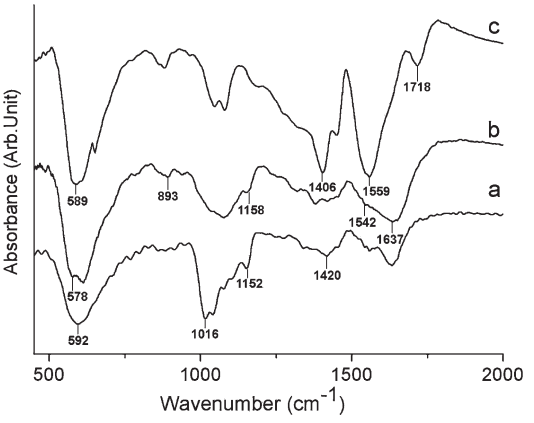

Figure 4. FTIR analysis of three types of MPPs. FTIR spectra of (a) DMMs, (b) CMMs, and (c) PMMs.

Fe_2O_3 while heat treating in air.[42,43] Thus, from the Raman spectra and TGA results of the three types of MPPs, it could be concluded that the crystalline form of them were γ-Fe_2O_3 but not Fe_3O_4. The magnetic properties of the samples were also investigated with a vibrating sample magnetometer. The microspheres showed excellent magnetotropism and dispersibility in water (Figure 3D). Saturation magnetization values were 35.42 $emug^{-1}$ for DMMs, 10.07 $emug^{-1}$ for CMMs, and 47.24 $emug^{-1}$ for PMMs. Moreover, the contents of the iron element in the three types of MPPs were 25.9% (DMMs), 19.65% (CMMs), and 29.4% (PMMs), respectively (Supplemental Figure 3 in the

(40) Thunemann, A. F.; Schutt, D.; Kaufner, L.; Pison, U.; Mohwald, H. *Langmuir* **2006**, *22*, 2351–2357.
(41) de Faria, D. L. A.; Silva, S. V.; de Oliveira, M. T. *J. Raman Spectrosc.* **1997**, *28*, 873–878.
(42) Zhan, S. H.; Chen, D. R.; Jiao, X. L.; Liu, S. S. *J. Colloid Interface Sci.* **2007**, *308*, 265–270.
(43) Rodulfo-Baechler, S. M.; Gonzalez-Cortes, S. L.; Orozco, J.; Sagredo, V.; Fontal, B.; Mora, A. J.; Delgado, G. *Mater. Lett.* **2004**, *58*, 2447–2450.

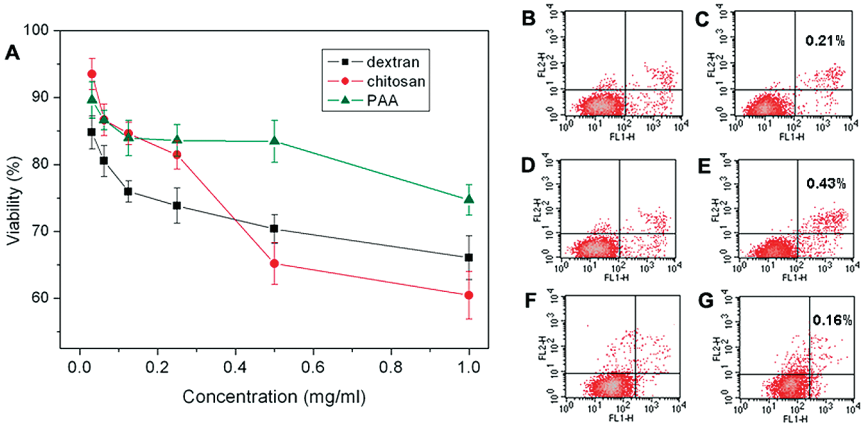

Figure 5. Effect of MPPs on cell proliferation and cell apoptosis. (A) Effect of MPPs on cell proliferation. (B−G) Effect of MPPs on cell apoptosis: (B, D, and F) controls not treated with MPPs and (C, E, and G) cells treated with DMMs, CMMs, and PMMs, respectively.

Supporting Information). Therefore, a possible explanation for the differences in saturation magnetization values is the different composition of the small magnetic nanocrystals in MPPs.

FTIR spectroscopy was used to confirm the functionalization of DMMs, CMMs, and PMMs by characterizing the properties of the functional groups on the surfaces of the three MPPs. FTIR spectra showed that DMMs had −OH groups (Figure 4a), CMMs had $-NH_2$ groups (Figure 4b), and PMMs had −COOH groups (Figure 4c). The strong FTIR bands present at 592 cm^{-1} (Figure 4a), 578 cm^{-1} (Figure 4b), and 589 cm^{-1} (Figure 4c) are characteristic of Fe−O vibrations. The main characteristic absorption band corresponding to DMMs is the free functionalized hydroxyl groups at 1016 cm^{-1}. Successful attachment of dextran was confirmed by the presence of a H−C−OH bond at 1420 cm^{-1} and a C−O−C bond at 1152 cm^{-1} (Figure 4a). Transmissions around 1542 and 893 cm^{-1} (Figure 4b) from the CMMs indicate the existence of free amino groups. Furthermore, the absorbance of C−O−C at 1158 cm^{-1} and −CONH at 1637 cm^{-1} also verified the presence of chitosan on the surface of the materials. The presence of free functionalized carboxyl groups was detected by a C═O bond at 1718 cm^{-1} and a C−O bond at 1406 cm^{-1} (Figure 4c). The peak at 1559 cm^{-1}, corresponding to the C═C bond, provided further confirmation of the attachment of PAA. Results from FTIR spectroscopy showed that functional groups on particle surfaces were provided by the polymer and that MPPs functionalized with different biodegradable polymers had been synthesized successfully.

Effect of MPPs on A375 Cells. To verify whether MPPs affected cellular activity, we prepared three types of MPPs with the same average size of 430 nm and incubated them with A375 cells. Cell viability was measured using the MTT assay. Cytotoxicity gradually increased with the MPP concentration for each of the three MPPs (Figure 5A). However, cell viability was still higher than 60% when the concentration of CMMs was as high as 1 mg/mL, sufficient for *in vivo* application.[44] Apoptosis and necrosis are both the pathways for cell death. To distinguish between apoptosis and necrosis induced by MPPs, a dual staining assay using annexin V and PI was applied. The apoptotic cells was determined using the positive staining of annexin V, and the late apoptosis or necrosis cells was demonstrated by positive staining of both annexin V and PI.[45] The positive staining of annexin V and PI demonstrated that DMMs, CMMs, and PMMs induced late apoptosis or necrosis of A375 cells (panels B−G of Figure 5). CMMs appeared more toxic than DMMs or PMMs in terms of cell viability and the percentage of late apoptosis or necrosis. This may be due to the effects of surface functional groups on MPPs; positively charged CMMs induce cell late apoptosis or necrosis more easily owing to the fact that cellular membranes are negatively charged.[46]

Intracellular Imaging of CMMs in A375 Cells. MNPs modified by polymers are excellent carriers for cellular labeling because of their easy control by magnetism and good biocompatibility.[47] Cellular imaging of CMMs was conducted by incubating FITC-labeled CMMs with A375 cells for 4 h. A375 cells exhibited green fluorescence throughout the whole cell (panels A−C of Figure 6). The lack of co-localization between CMM (green) and DAPI (blue) fluorescence indicates that the CMMs are not localized to the nucleus but rather are distributed throughout the cytoplasm (Supplemental Figure 4 in the Supporting Information). Because FITC alone is impermeable,[48] we can conclude that the FITC that penetrated the plasma membrane was carried by CMMs and thus delivered into the cytoplasm. CMMs labeled with FITC and LysoTracker Blue DND-22 were incubated with A375 cells at 37 °C to determine whether nanoparticles carrying biomolecules could move out of the lysosome into the cytoplasm or nucleus to avoid degradation by the nucleases and proteinases that are present in the lysosome.[49−52] FITC-labeled CMMs were observed in the lysosomes (panels D−F of Figure 6); however, about 50% of the cells displayed green fluorescence throughout the cell (arrow in Figure 6F), indicating that CMMs were able to move out of the lysosome into the cytoplasm. These results indicate that CMMs are potential carriers for intracellular imaging and drug delivery.

Antibody Purification Using PMMs. Owing to the controllability of MNPs, they are considered as excellent carriers for protein purification. Proteins can readily be covalently coupled to nanoparticles with −COOH groups that possess high labeling

(44) Tang, N.; Du, G.; Wang, N.; Liu, C.; Hang, H.; Liang, W. *J. Natl. Cancer Inst.* **2007**, *99*, 1004–1015.
(45) Zhao, J.; Bowman, L.; Zhang, X.; Shi, X.; Jiang, B.; Castranova, V.; Ding, M. *J. Nanobiotechnol.* **2009**, *7*, 2.
(46) Nabiev, I.; Mitchell, S.; Davies, A.; Williams, Y.; Kelleher, D.; Moore, R.; Gun'ko, Y. K.; Byrne, S.; Rakovich, Y. P.; Donegan, J. F.; Sukhanova, A.; Conroy, J.; Cottell, D.; Gaponik, N.; Rogach, A.; Volkov, Y. *Nano Lett.* **2007**, *7*, 3452–3461.
(47) Babic, M.; Horak, D.; Trchova, M.; Jendelova, P.; Glogarova, K.; Lesny, P.; Herynek, V.; Hajek, M.; Sykova, E. *Bioconjugate Chem.* **2008**, *19*, 740–750.
(48) Lencer, W. I.; Weyer, P.; Verkman, A. S.; Ausiello, D. A.; Brown, D. *Am. J. Physiol.* **1990**, *258*, 309–317.
(49) Liu, Y.; Wenning, L.; Lynch, M.; Reineke, T. M. *J. Am. Chem. Soc.* **2004**, *126*, 7422–7423.
(50) Sokolova, V.; Epple, M. *Angew. Chem., Int. Ed.* **2008**, *47*, 1382–1395.
(51) Je, J. Y.; Cho, Y. S.; Kim, S. K. *Biomacromolecules* **2006**, *7*, 3448–3451.
(52) Dobson, J. *Gene Ther.* **2006**, *13*, 283–287.

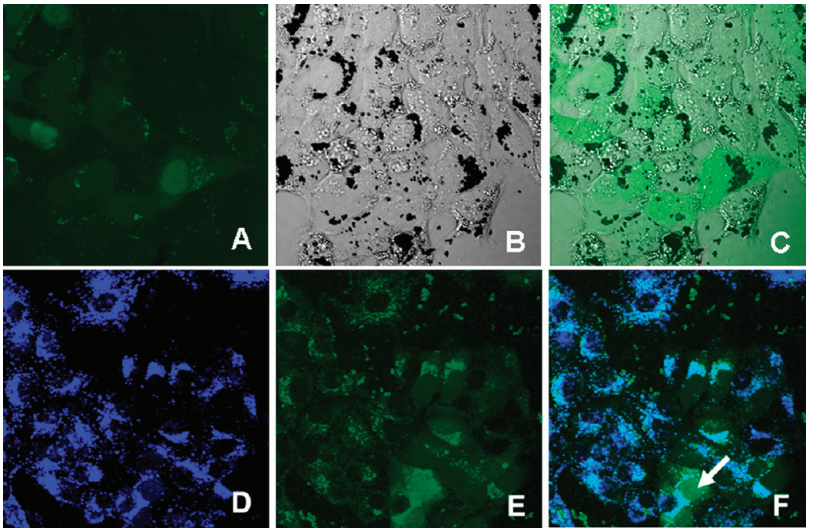

Figure 6. Intracellular imaging of FITC-labeled CMMs in A375 cells. (A) Fluorescent, (B) bright, and (C) merge images of FITC-labeled CMMs taken up by A375 cells, indicating that CMMs were mainly distributed in the cytoplasm. (D) Lysosomes in A375 cells. (E) Fluorescence image of FITC-labeled CMMs taken up by A375 cells. (F) Co-localization of the CMMs and lysosomes (white). Many cells showed surplus green fluorescence (arrow), indicating that CMMs escaped from lysosomes into the cytoplasm.

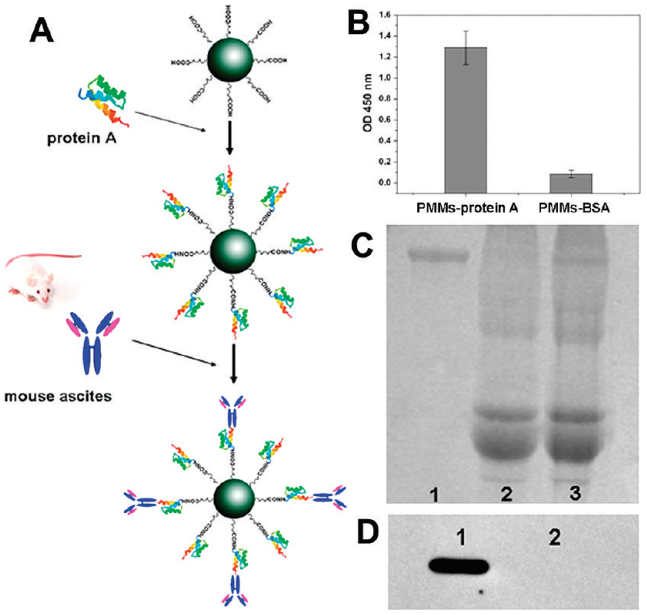

Figure 7. Usage of PMMs for antibody purification. (A) Antibody purification involved two steps: (1) PMMs were covalently coupled with protein A, and (2) antibodies in mouse ascites were captured by protein-A-labeled PMMs. (B) Direct ELISA was used for analyzing the bioactivity of protein A in protein-A-labeled PMMs. First, mIgG was coated on ELISA plates, and then protein-A-labeled PMMs or BSA-blocked PMMs were added. Protein A in the protein-A-labeled PMMs retained its bioactivity. (C) SDS−PAGE of antibody purification by protein-A-labeled PMMs. The covalently coupled protein A on the PMMs acted as an antibody purification vector: (1) purified antibody, (2) surplus mouse ascites after purification, and (3) mouse ascites before purification. (D) Western blotting showing the activity of the purified antibody. The lysate of LS174T was transferred onto the nitrocellulose membrane and (1) purified antibody or (2) PBS was added to detect whether the purified antibody could specifically recognize the antigen.

efficiency. Here, PMMs were covalently coupled with protein A by EDC/NHS and used for antibody purification from mouse ascites (Figure 7A). The labeling efficiency of PMMs coupled with protein A was above 80% (data not shown). To demonstrate that protein A maintained its activity when attached to PMMs, HRP-labeled goat-anti-mouse IgG was added to PBS containing the protein-A-labeled PMMs. BSA-blocked naked PMMs were used as a negative control. Our results showed that protein A could capture HRP-labeled goat-anti-mouse IgG successfully, which indicated the bioactivity of protein A was retained after its attachment to PMMs (Figure 7B). Protein-A-labeled PMMs were then used successfully to capture anti-CEA monoclonal antibody from mouse ascites (lane 1 in Figure 7C). It is important that the activity of the purified antibody is not affected during the purification process.[53] Western blotting results verified that the purified antibody could still recognize its antigen (CEA), a protein of 130 kDa, in the lysate of human epithelial colon cell line LS174T (Figure 7D). In comparison to the long operation time, solvent consumption, and problems with protein solubility associated with affinity chromatography,[54] the conventional method for antibody purification, we have demonstrated that use of PMMs is a much simpler and more versatile system for antibody purification.

Conclusion

In this paper, a simple, general strategy for the preparation of a range of functionalized, hydrophilic, monodispersible, and biocompatible MPPs was developed by selecting different polymers as surfactants in the one-pot synthesis reaction system. Biomolecules were attached to these functionalized MPPs, which were then used for intracellular imaging and antibody purification. We showed that the functional groups of MPPs played a significant role in creating multifunctionalities and catering for different bioapplications. Our results indicated that MPPs had only a slight influence on cell proliferation and viability, showing low cytotoxicity, and excellent biocompatibility. In summary, the simple and general synthesis strategy described here, using different polymers as a source of functional groups, is an effective method with promising potential for designing multifunctional nanomaterials with wide biological

(53) Park, H. Y.; Schadt, M. J.; Wang, L.; Lim, I. I.; Njoki, P. N.; Kim, S. H.; Jang, M. Y.; Luo, J.; Zhong, C. J. *Langmuir* **2007**, *23*, 9050–9056.
(54) Xu, C.; Xu, K.; Gu, H.; Zhong, X.; Guo, Z.; Zheng, R.; Zhang, X.; Xu, B. *J. Am. Chem. Soc.* **2004**, *126*, 3392–3393.

and medical applications arising from their hydrophilicity, monodispersion, biocompatibility, and surface functionalization.

Acknowledgment. The authors acknowledge financial support from the National Hi-Technology Research and Development Program (863 Program) (2007AA021802 and 2007AA021803) and the National Natural Science Foundation (30800258 and 20873171).

Supporting Information Available: TEM images of MPPs synthesized using different polymers as surfactants in the one-pot synthesis reaction system (Supplemental Figure S1), relationship between the quantity of polymer used in the one-pot synthesis reaction system and reaction time in the monodispersion of MPPs (Supplemental Figure S2), images of intracellular trafficking with FITC-labeled CMMs in A375 cells (Supplemental Figure S3), and relationship between average sizes of MPPs and reaction time or concentration of reactants (Supplemental Table S1). This material is available free of charge via the Internet at http://pubs.acs.org.